Open Access Full Text Article

ORIGINAL RESEARCH

Investigating the Potency of Erythrina–Derived Flavonoids as Cholinesterase Inhibitors and Free Radical Scavengers Through in silico Approach: Implications for Alzheimer's Disease Therapy

Abd Wahid Rizaldi Akili[1], Nisrina Azizah Thurfah[1], Ari Hardianto[1], Jalifah Latip[2], Tati Herlina[1]

[1]Department of Chemistry, Faculty of Mathematics and Natural Science, Universitas Padjadjaran, Sumedang, West Java, 45363, Indonesia; [2]Department of Chemical Sciences, Faculty of Science and Technology, Universiti Kebangsaan Malaysia (UKM), Bangi, Selangor, 46300, Malaysia

Correspondence: Tati Herlina, Email tati.herlina@unpad.ac.id

Purpose: This study aimed to evaluate the potency of 471 flavonoids from the genus *Erythrina* as potential acetylcholinesterase (AChE) inhibitors and free radical scavengers through computational studies to develop Alzheimer's disease (AD) therapies from natural products.

Methods: A total of 471 flavonoids from the genus *Erythrina* were subjected to molecular docking against AChE, followed by toxicity screening. The potential AChE inhibitors with the least toxic profile were subjected to further investigation through molecular dynamics (MD) simulations, density functional theory (DFT) study, and in silico pharmacokinetic predictions.

Results: A combination of molecular docking and in silico toxicity screening led to the identification of 2(S)–5,7–dihydroxy–5′–methoxy–[2″,2″–(3″–hydroxy)–dimethylpyrano]–(5″,6″:3′,4′) flavanone (89) and Abyssinoflavanone IV (83) as potential AChE inhibitors. These compounds had stable binding to AchE and exhibited lower Root Mean Square Deviation (RMSD) values compared to the apo state of AChE. In addition, Molecular Mechanics Generalized Born Surface Area (MMGBSA) analysis revealed that the binding energies of 89 and 83 were significantly lower compared to acetylcholine, the natural substrate of AChE. Based on DFT study, these compounds exhibited a higher energy in the highest occupied molecular orbital (E_{HOMO}) and lower electron affinity (EA) than Quercetin. This indicated that 89 and 83 could be potential radical scavengers through their electron-donating activity.

Conclusion: Although this study primarily relied on computational methods, the results showed the dual functionality of compounds 89 and 83 as both potential AChE inhibitors and free radical scavengers. Further investigation in wet laboratory experiments is required to validate their therapeutic potential for AD.

Keywords: flavonoids, erythrina, acetylcholinesterase, free radical scavenger, in silico

Introduction

Alzheimer's disease (AD) poses a significant global health challenge, affecting millions of people worldwide, with its prevalence increasing as age advances.[1] Several studies have shown that therapeutic interventions play a crucial role in addressing the cognitive decline associated with AD. During the treatment process, cholinesterase (ChE), including acetylcholinesterase (AChE) and butyrylcholinesterase (BuChE), serves as key molecular targets.[2] These enzymes are responsible for acetylcholine hydrolysis, which is essential for memory and cognitive functions. In addition, inhibition of ChE can elevate acetylcholine levels, potentially enhancing cholinergic neurotransmission and mitigating cognitive deficits in AD patients.[3]

The formation of free radical species is another important neurotoxic pathway in the development of AD.[4] As individuals age, the formation and accumulation of free radical species in the body exacerbates oxidative stress and weakens cellular antioxidant defense mechanisms.[5] Numerous studies have shown that antioxidants can either prevent or

Received: 15 August 2024
Accepted: 15 October 2024
Published: 1 November 2024

ameliorate AD.[6–8] Therefore, the discovery and development of medicinal compounds possessing both antioxidant and anti-ChE activities are essential for effective treatment.[9]

In line with these results, flavonoids are a diverse class of polyphenolic compounds found abundantly in fruits, vegetables, and medicinal plants.[10] Flavonoids are recognized for their broad spectrum of health-promoting properties, including antioxidant and anti-inflammatory activities. In addition, these compounds have been extensively studied due to their potential therapeutic applications.[11] Flavonoids have also shown significant potential as anti-ChE agents and ChE activity inhibitors.[12,13] For instance, compounds isolated from *Dorstenia* and *Polygonum* genus showed inhibitory activity against AChE, with IC_{50} values ranging from 5.93 to 8.75 µg/mL.[14]

The genus *Erythrina* has been reported to comprise medicinal plants rich in flavonoids, with approximately 471 compounds being isolated.[15,16] Several studies revealed that extracts from various *Erythrina* species, including *E. corallodendron*,[17] *E. caffra*,[18] *E. velutina*[19] and *E. variegata*[20] have the potential to serve as therapeutic agents for AD by inhibiting AChE enzyme activity. However, there is no available literature on the potency of flavonoids derived from the genus *Erythrina* as AChE inhibitors.

In silico approaches, such as molecular docking and dynamic simulations, offer a powerful method to explore ligand-receptor interactions at the atomic level.[21] Therefore, this study aims to determine the binding affinity, binding mode, and stability of flavonoids from the genus *Erythrina* with AchE using computational tools. Potential lead compounds were also identified for further experimental validation by elucidating the structural basis of flavonoid–AChE interactions. The results of this study are expected to bridge the gap between natural product chemistry and computational biology, providing insights into the therapeutic potential of flavonoids from the genus *Erythrina* as ChE inhibitors to combat AD.

Materials and Methods

Molecular Docking System Preparation

The 3D X-ray crystal structure of human AChE in complex with galantamine (GNT) was downloaded from Protein Data Bank (PDB) (https://www.rscb.org, accessed on April 25th, 2024) with PDB ID of 4EYH. Furthermore, co-crystallized ligand was separated from the 3D structure of the protein and saved in PBD format, while the water molecules were removed from the ligand-free protein and saved in PDB format. Both the ligand and protein were processed using AutoDock tools (version 1.5.7), and saved in the pdbqt format.

In this study, the structures of the 471 flavonoids were retrieved from several literature reviews.[15,16] The protonated state of these flavonoids was predicted using Chemaxon MarvinSketch, and the 3D structures were optimized using the Merck molecular force field (MMFF94) and saved in the format. Finally, the 3D structures were further processed using AutoDock tools (version 1.5.7), and saved in pdbqt format.[22]

Redocking and Virtual Screening

The prepared protein and co-crystallized ligand structures were subjected to a redocking procedure using AutoDock Vina (version 1.2.0). In addition, the grid box parameter was set to a size of 36×36 x 40 with a 0.375 Å spacing, which covered co-crystallized ligand and the largest flavonoid structure for docking. The docking poses generated by AutoDock Vina were separated using Vina Split, and the most preferred pose (with the lowest binding score) was superimposed onto co-crystallized ligand file. Subsequently, Root Mean Square Deviation (RMSD) was calculated using Biovia Discovery, which resulted in RMSD of 0.3403 Å. The docking parameters from redocking procedure were then applied to virtual screen 471 flavonoids against the human AChE protein.

Molecular Dynamics (MD) Simulation

According to previous studies, MD simulation for the best-hit compound was conducted using Amber20 with GPU acceleration.[23,24] The amino acid residues of AChE were parameterized using the ff19SB force field. Furthermore, the partial atomic charges of the ligands were determined using the Austin Model 1–Bond Charge Corrections (AM1–BCC) method in the antechamber module of Amber–Tools21. Additional parameters for the ligand were sourced from the generalized amber force field 2 (GAFF2). AChE–ligand complex was solvated using the tleap module in Amber-Tools21,

with solvent box dimensions of 10 Å. In addition, a small number of Na^+ and Cl^- ions were added to the system to achieve a 0.15 M salt concentration.

The simulation process began with 2 consecutive energy minimization steps. For the protein-ligand complex, a restraint of 25 kcal $mol^{-1}Å^{-2}$ was applied in the initial step, followed by 5 kcal $mol^{-1}Å^{-2}$ in the second step of minimization. After the minimization step, the temperature of the system was increased to 300 K under a 50–ps NVT (Number–Volume–Temperature) condition and then switched to Number–Pressure–Temperature (NPT) condition. Subsequently, the system density was adjusted to 1 $g.cm^{-3}$ over a 50–ps period. During subsequent NVT simulations, the restraint on the solute was gradually reduced by 1 kcal mol^{-1} $Å^{-2}$ every 50 ps until it was fully eliminated.

In this study, the system was simulated at a temperature of 300 K under NPT conditions to produce a 100–ns MD trajectory. Particle–Mesh Ewald (PME) method was used to overcome long-range electrostatic interactions, while a 10–Å cut–off was applied for short–range non–bonded interactions. A SHAKE algorithm was used to maintain bond constraints, including hydrogen atoms. Simultaneously, the temperature and pressure of the system were controlled using a Langevin thermostat and Berendsen barostat, respectively.[23,24]

Density Functional Theory (DFT) Study

Molecular structures of the hit compound and quercetin (used as a standard antioxidant) were optimized using DFT with the B3LYP method and the 6–311G++(d,p) basis set in the Gaussian 09 software. Following the optimization, vibrational frequency analysis confirmed that no imaginary frequencies were present in the optimized structures.[25]

The global descriptive parameters, including the ionization potential (I), electron affinity (A), hardness (η), softness (S), electronegativity (χ), chemical potential (μ), electrophilicity index (ω), electron-donating power (ω–), and electron accepting power (ω+), were calculated based on the vertical energy method using the following equations:[26]

$$I = E_{cation} - E_{neutral}$$

$$A = E_{neutral} - E_{anion}$$

$$\eta = \frac{(I - A)}{2}$$

$$\chi = \frac{(I + A)}{2}$$

$$s = \frac{1}{2\eta}$$

$$\mu = -\chi$$

$$\omega = \frac{\mu^2}{2}$$

$$\omega^- = \frac{(3I + A)^2}{16(I - A)}$$

$$\omega^+ = \frac{(I + 3A)^2}{16(I - A)}$$

In silico Pharmacokinetics Prediction

The ADMETlab 2.0 web server (https://admetmesh.scbdd.com, accessed on May 3, 2024) was used to predict the pharmacokinetic properties (absorption, distribution, metabolism, and excretion) of the potential AChE inhibitor.

Table 1 List of 9 AChE Inhibitor Hits

Flavonoid Name	Flavonoid Subclass	Docking Score (Kcal/mol)
Abyssinin I (80)	Flavanone	–11.1
Abyssinoflavanone IV (83)	Flavanone	–11.24
Abyssinoflavanone VI (85)	Flavanone	–10.66
2(S)–5,7–dihydroxy–5′–methoxy–[2″,2″–(3″–hydroxy)– dimethylpyrano]–(5″,6″:3′,4′) flavanone (89)	Flavanone	–11.36
(2S)–5,7–dihydroxy–5′–methoxy–2″–(4″–hydroxyisopropyl)– dihydrofurano[1″,3″:3′,4′] flavanone (95)	Flavanone	–10.57
Erypoegin A (Burttinol C) (139)	Isoflav–3–ene	–10.81
Vogel (387)	Flavone	–10.65
Dihydroxyabyssin (400)	Flavanone	–11.02
Erydroogmansin A (425)	Isoflavanone	–10.9
Galantamine	Inhibitor	–10.44

Results

Molecular Docking and Toxicity Screening

Molecular docking was used to screen the binding affinity of 471 flavonoids isolated from the genus *Erythrina* for AChE, with galantamine as the standard. Out of the 471 flavonoids, 88 exhibited lower docking scores compared to that of galantamine which exhibited docking score of −10.44 kcal/mol as cutoff (Table S1). These potential AChE inhibitors were evaluated for toxicity (Table S2), and 9 of these flavonoids showed a low to medium risk of toxicity and were listed in Table 1. Among these flavonoids, 2(S)–5,7–dihydroxy–5′–methoxy–[2″,2″–(3″–hydroxy)–dimethylpyrano]–(5″,6″:3′,4′) flavanone (89) and Abyssinoflavanone IV (83) (Figure 1) are the top hits which were further subjected to MD simulation, DFT study and pharmacokinetics prediction.

Molecular Dynamics (MD) Simulation

Among these 9 hits, the first 2 were evaluated for further analysis using MD. The results could be described in terms of RMSD, Root Mean Square Fluctuation (RMSF), and Molecular Mechanics Generalized Born Surface Area (MMGBSA) free energy.

RMSD

RMSD plots of the Apo form, along with AChE–89 and AChE–83 complexes, were shown in Figure 2. The apo state of AChE exhibited the highest RMSD, with a median value of 1.783 Å and a median absolute deviation (MAD) of 0.321 Å. Both AChE–83 and AChE–89 complexes displayed the lowest RMSD (median = 1.525 Å, MAD = 0.114 Å and median = 1.558 Å, MAD = 0.126 Å, respectively) when compared to AChE–GNT and AChE–ACh complexes (Table S3).

RMSF

RMSF profiles of AChE–89 and AChE–83 complexes and the Apo form of AChE were shown in Figure 3. On close inspection of the 100 ns trajectories within several structural regions, including the triad, omega loop, and George entry, significant differences emerged between the apo (unbound) and ligand-bound forms of AChE. The amino acid residues in the triad, omega loop, and George entry exhibited lower B–factors in the ligand-bound complex compared to the apo

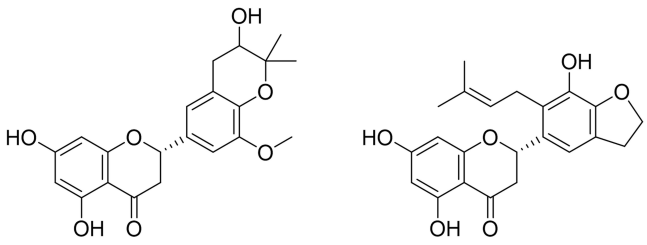

Figure 1 Chemical structure of compounds 89 (left) and 83 (right).

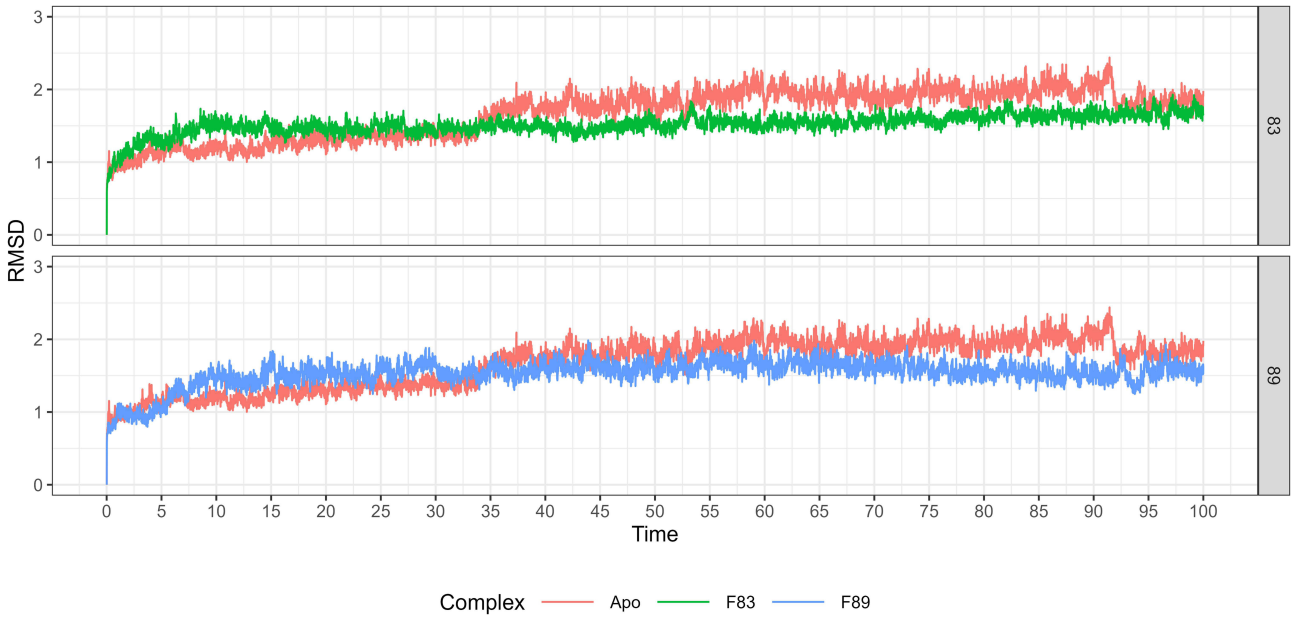

Figure 2 RMSD plot comparison of Apo AChE Vs AChE– 83 complex (green) and AChE– 89 complex (blue).

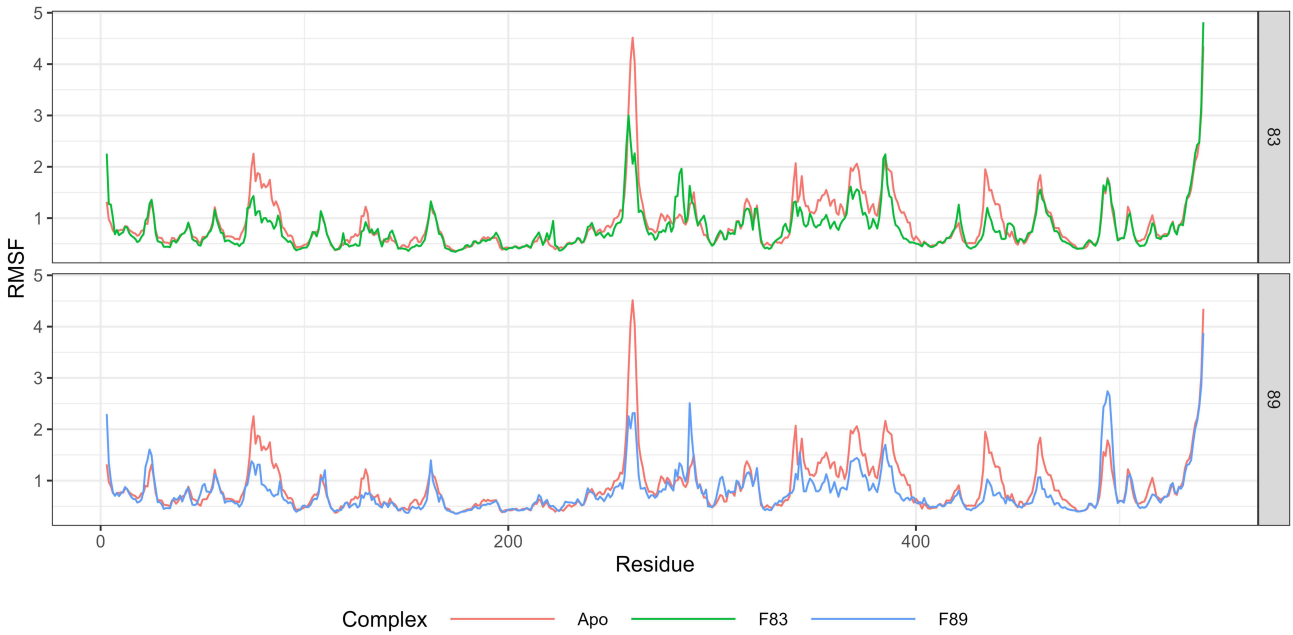

Figure 3 RMSF plot comparison of Apo AChE Vs AChE– 83 complex (green) and AChE– 89 complex (blue).

form of AChE (Table S4). This observation suggested that amino acids in these structural regions were more stable and exhibited less movement.

MMGBSA Free Energy Calculation

MMGBSA Analysis was a computational method extensively used in MD simulations to investigate binding affinities and interactions between molecules.[27] The ΔG^{o}_{MMGBSA} calculation from MD simulation trajectories revealed that galantamine (a well-known AChE inhibitor) had the lowest binding energy, followed by compounds 89, 83 and acetylcholine (a native substrate of AChE) (Table 2).

Table 2 $\Delta g^{\circ}_{mmgbsa}$ Values of Acetylcholine–, Galantamine–, 89–, and 83–AChE Complex (Expressed as Median ± SD)

Ligand	$\Delta G^{\circ}_{MMGBSA}$ (Kcal/mol)	$\Delta G^{\circ}_{MMGBSA}$ Energy Terms (Kcal/mol)			
		vdW	Electrostatics	EGB	ESurf
Galantamine	–42.85 ± 10.20	–36.64 ± 0.84	–39.03 ± 17.14	32.86 ± 8.02	–4.78 ± 0.24
89	–37.94 ± 5.69	–46.97 ± 2.69	–28.10 ± 7.51	42.17 ± 4.75	–5.80 ± 0.15
83	–32.93 ± 2.26	–46.99 ± 2.03	–28.57 ± 11.39	49.37 ± 9.69	–5.86 ± 0.17
Acetylcholine	–24.33 ± 3.56	–22.90 ± 1.37	–270.44 ± 5.94	272.76 ± 5.29	–3.36 ± 0.42

To evaluate whether there was a significant difference between the 4 complexes, Kruskal–Wallis rank-sum test was performed. Furthermore, the test was followed by Dunn's multiple-comparison test, using the Bonferroni method as a post–hoc test.[23] The test suggested that there was no statistical difference between the $\Delta G^{\circ}_{MMGBSA}$ values of galantamine and both 89 and 83. However, both were significantly different from that of acetylcholine (Figure 4); therefore, compounds 89 and 83 were identified as potential AChE inhibitors.

Density Functional Theory (DFT)

According to previous studies on other flavonoid compounds, DFT study was conducted to evaluate the free–radical scavenging potency of 89 and 83. The global descriptive parameters, including E_{HOMO}, E_{LUMO}, ΔE_{gap}, ionization potential (I), electron affinity (A), hardness (η), softness (σ), electronegativity (χ), chemical potential (μ), electrophilicity index (Ω), electron-donating power (ω^{-}), and electron–accepting power (ω^{+}), were used to assess the reactivity of 89 and 83 toward free radicals in comparison with Quercetin (a well–known antioxidant) as a standard. The global descriptive parameter values for 89, 83, and Quercetin were listed in Table 3.

In silico Pharmacokinetics Prediction

Pharmacokinetic prediction was a crucial aspect of drug design and discovery, as it allowed for early estimation of the absorption, distribution, metabolism, and excretion (ADME) properties of potential drug candidates. This early

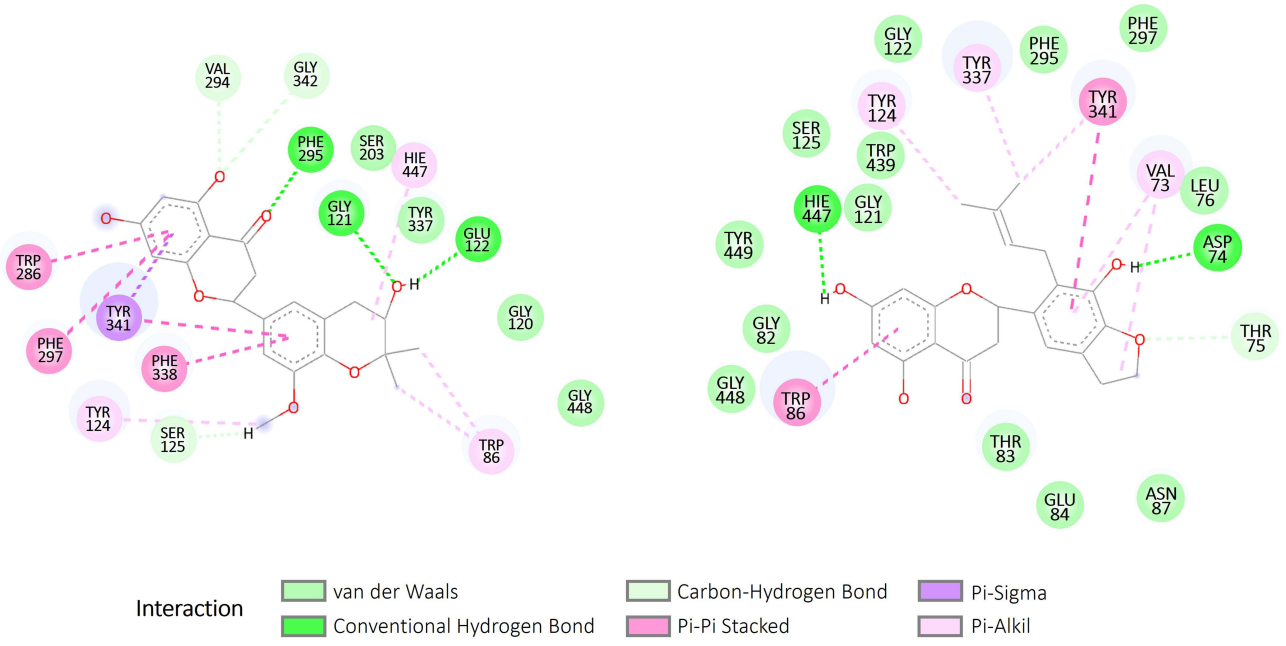

Figure 4 The 2D representation of 89 (left) and 83 (right) interaction with active site of AChE.

Table 3 Global Descriptive Parameter of Compound 89 and Quercetin as Standard

Global Descriptive Parameter	Value (eV)		
	89	83	Quercetin
E_{HOMO}	–0.21835	–0.22195	–0.22311
E_{LUMO}	–0.05502	–0.0593	–0.07586
ΔE_{gap}	–0.16333	–0.16265	–0.14725
Ionization potential (I)	7.38354023	7.43831677	7.54223709
Electron affinity (A)	0.05825960	0.00087076	0.62493692
Hardness (η)	3.662640314	3.718723001	3.458650083
Softness (σ)	0.136513541	0.134454758	0.144565073
Electronegativity (χ)	3.720899913	3.719593766	4.083587006
Chemical potential (μ)	–3.720899913	–3.719593766	–4.083587006
Electrophilicity index (Ω)	6.92254808	6.917688891	8.337841418
Electron donating power (ω^-)	4.208323103	4.184869625	4.884846062
Electron accepting power (ω^+)	0.48742319	0.465275859	0.801259056

estimation significantly reduced the fraction of pharmacokinetics-related failures in the clinical phase, which eventually enhanced the efficiency of drug development.[28] Therefore, after evaluating the potency of compound 89 as AChE inhibitor and radical scavenger, pharmacokinetic prediction of 89 and 83 was performed, and the results were summarized in Table 4.

Table 4 Pharmacokinetics Prediction of Compounds 89 and 83

Pharmacokinetic Properties	Parameters	Predicted Values		Unit
		89	83	
Absorption	Caco–2 permeability	–4.848	–4.908	log cm/s
	MCDK permeability	1.3×10^{-5}	1.2×10^{-5}	cm/s
	Pgp–inhibitor	Yes	Yes	–
	Pgp–substrate	No	No	–
	Human intestinal absorption	>30	>30	%
Distribution	Plasma Protein Binding	92.15	97.35	%
	Volume Distribution	1.027	0.637	L/kg
	BBB Penetration	Yes	Yes	–
	Fraction unbound	8.02	3.59	%
Metabolism	CYP1A2 inhibitor	No	Yes	–
	CYP1A2 substrate	No	No	–
	CYP2C19 inhibitor	No	Yes	–
	CYP2C19 substrate	No	Yes	–
	CYP2C9 inhibitor	Yes	Yes	–
	CYP2C9 substrate	Yes	Yes	–
	CYP2D6 inhibitor	Yes	Yes	–
	CYP2D6 substrate	No	No	–
	CYP3A4 inhibitor	Yes	Yes	–
	CYP3A4 substrate	No	No	–
Excretion	Drug clearance	13.419	16.486	mL/min/kg
	Half–life	0.393	0.485	–

Discussion

Out of the 471 flavonoids evaluated, 9 hits were identified with lower binding affinities compared to that of galantamine (GNT) and were predicted to exhibit low to medium toxicity. The top 2 hits, namely 2(S)–5,7–dihydroxy–5′–methoxy–[2′′,2′′–(3′′–hydroxy)–dimethylpyrano]–(5′′,6′′:3′,4′) flavanone (89) and Abyssinoflavanone IV (83) (Figure 1) were further subjected to MD simulation to evaluate the stability of AChE upon binding to these compounds. This was followed by in silico pharmacokinetics and drug-likeness prediction to evaluate the potency of these compounds to be developed as potential drugs for AD therapy.

RMSD was a crucial metric for studying biomolecules during simulations and experiments. It quantified the average displacement of atoms from their initial positions and could provide insights into the dynamic behavior of a biomolecule as it interacted with other molecules (*eg*, a docked ligand). RMSD plot (Figure 2) indicated that both 89 and 83 stabilized AChE protein, as both AChE–83 and AChE–89 complexes displayed the lowest RMSD (median = 1.525 Å, MAD = 0.114 Å and median = 1.558 Å, MAD = 0.126 Å, respectively). A lower RMSD value indicated greater stability of the biomolecular structure during these interactions.[29] As comparison, RMSD values of both 83 and 89 were lower compared to that of AChE-quercetin complex in the literature (1.9 Å). Furthermore, it was noteworthy that Quercetin exhibited inhibitory activity against AChE with IC_{50} of 4.59 ± 0.27 µM.[30] The stability of both AChE–83 and AChE–89 complexes was further supported by RMSF plot (Figure 3). RMSF quantified these fluctuations by calculating RMSD of the atomic positions from their equilibrium positions.[31] RMSF plot served as a common representation of residues that had undergone substantial changes during MD simulation.[32] For all AChE–ligand complexes, except for the C-terminus and N-terminus, the other residues in AChE did not fluctuate significantly, including in the triad, omega loop, and George entry.

A 2D graphical representation of the interaction of AChE with 89 and 83 was shown in Figure 4. At the catalytic or acylation site of AChE, compound 89 interacted with His^{447} through Pi-Alkil, while compound 83 interacted with the same amino acid residue through a conventional hydrogen bond. The catalytic or acylation site comprised 3 essential amino acid residues (*such as* Ser^{203}, His^{447}, and Glu^{334}). Each of these amino acid residues played a crucial role in the hydrolysis of acetylcholine. Ser^{203} acted as a nucleophile during substrate hydrolysis, His^{447} stabilized the transition state during the acylation process, and Glu^{334} assisted in substrate binding and catalysis.[33] Because 89 and 83 could interact with His^{447}, these compounds could interrupt the catalytic function of AChE. Moreover, in the "anionic" subsite, compound 89 interacted with Trp^{86} and Phe^{338}, while compound 83 interacted with both Trp^{86} and Tyr^{337}. These amino acid residues played important roles in the binding and stabilization of the substrate in the active site as it was bound to the quaternary trimethylammonium choline moiety.[34]

MMGBSA free energy calculations indicated that both 89 and 83 had significantly lower binding energies than ACh, which was the natural substrate of AChE. Although both 89 and 83 had higher binding energies than galantamine (a known AChE inhibitor), the median difference in binding energy during the 100 ns simulation was not significantly different (Figure 5). This result suggested that the binding of 89 or 83 was more favorable than that of ACh; therefore, inhibitory activity against AChE could be exhibited. As comparison with available literature data, the ΔG_{bind} of both 89 and 83 are lower than that of Quercetin (ΔG_{bind} = −21.0 ± 2.5 Kcal/mol)[35] which further support the potential inhibitory activity of 89 and 83 against AChE.

In terms of free radical scavenging activity, the global descriptive parameter values of 89 and 83 were close to those of the Quercetin. However, in terms of electron affinity (EA) and electron-accepting power (ω^+), the values were quite different. EA corresponded to the energy released when a neutral molecule captured an electron. The higher the EA value, the better the ability of a neutral molecule to accept electrons from a radical, thereby suggesting better radical scavenging activity.[36] Furthermore, EA of Quercetin was much higher than those of 89 and 83, implying that the Quercetin had a better ability to accept electrons compared to 89 and 83. Quercetin had a higher electron–accepting power (ω^+) than 89 and 83, which further supported the better ability of Quercetin to accept electrons. However, the higher E_{HOMO} and lower EA of 89 and 83 suggested that both compounds were good electron donors compared to quercetin. In this study, 89 and 83 could be potential radical scavengers owing to their electron–donating activities.

Based on the results of MD simulation and DFT study, it was evident that 89 and 83 could be potential AChE inhibitors as well as free radical scavengers. Therefore, in the next step, in silico pharmacokinetic studies were conducted to predict the pharmacokinetic properties of 89 and 83. Pharmacokinetics referred to the study of how drug

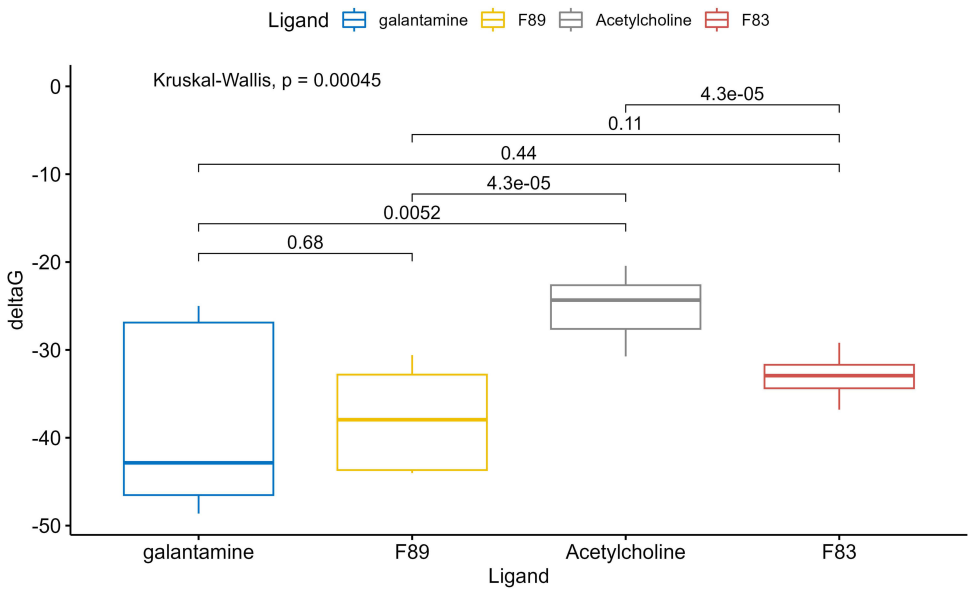

Figure 5 Box Plots of ΔG°MMGBSA for ligand binding AChE with significant test results from a Dunn test, a post hoc of Kruskal–Wallis rank sum test.

concentrations change over time following drug administration. This included processes, such as absorption, distribution, metabolism, and excretion (ADME).[22]

Drug absorption was a critical aspect of pharmacokinetics that comprised the process by which a drug entered the bloodstream to exert its therapeutic effect.[37] In terms of drug absorption parameters, the prediction model suggested that both 89 and 83 exhibited high Caco-2, which were the human intestinal epithelial cells and MCDK permeability. High Caco-2 permeability indicated that a compound could readily cross the intestinal barrier and be absorbed into the systemic circulation. Meanwhile, a high MDCK permeability implied that a compound could traverse the renal tubular epithelium efficiently. Compounds with high Caco-2 and MDCK permeability were likely to be well–absorbed and efficiently eliminated, making these compounds favorable candidates for drug development.[38] The prediction model also suggested that 89 and 83 were not substrates of P–gp but could serve as P-glycoprotein (P–gp) inhibitors. This result implied that the bioavailability of these compounds was not affected by P-gp activity, which acted as an efflux transporter and actively pumps xenobiotics into the lumen of the small intestine.[24]

Pharmacokinetics drug distribution referred to the reversible transfer of a drug between different compartments of the body. Once the drug entered systemic circulation through absorption or direct administration, it was distributed in both interstitial and intracellular fluids.[22] Based on the prediction model, 89 and 83 were reported to have a good volume distribution with a value of 0.04–20 L/kg. Blood-brain barrier (BBB) permeability was another parameter used to describe drug distribution in the human body. BBB was a selective, semi-permeable membrane composed of tight junctions. Furthermore, it served as a protective barrier that limited the entry of specific substances from the bloodstream into the central nervous system (CNS). When a drug crossed the BBB, it gained access to the brain tissue. This ability was essential for treating CNS disorders (eg AD and epilepsy). The prediction model suggested that 89 and 83 could cross BBB. The unbound fraction represented the proportion of free drugs in the plasma. It was the fraction of drug molecules that were not bound to plasma proteins (such as albumin). Only the unbound drug could be distributed to the tissues, while the bound drug remained in the bloodstream. The prediction model suggested that compound 89 had a medium unbound fraction. Nevertheless, both 89 and 83 were predicted to exhibit high plasma protein binding (>90%), which could have a slower elimination rate, affecting the dosing intervals.

In terms of drug metabolism, the prediction model suggested that 89 and 83 could act as CYP2C9 substrates, indicating that these compounds could be metabolized by this specific enzyme. In the human liver, was the predominant enzyme within the CYP2C subfamily and played a crucial role in metabolizing clinically relevant drugs in a narrow therapeutic range.[39]

The drug excretion properties of 89 and 83 were evaluated in terms of drug clearance and half-life. Drug clearance represented the elimination rate of a substance divided by its concentration, and reflected the theoretical plasma volume from which the substance was entirely removed per unit of time. The prediction model suggested that compound 89 had moderate clearance, indicating that 89 was eliminated from the body at a moderate rate, and suggested a balance between rapid elimination and prolonged presence in the bloodstream. Meanwhile, 83 was predicted to have a high clearance, indicating that it could be eliminated from the body at a higher rate.

The half-life ($T_{1/2}$) represented the estimated time, which was required for its concentration or amount in the body to decrease to 50% of its initial concentration (50%). The prediction model suggested that compound 89 had a half-life lower than 83, suggesting that it could remain in the body for a longer duration before being eliminated compared to 89.

Conclusion

In conclusion, through a combination of molecular docking, in silico toxicity screening had led to the identified 2(S)-5,7-dihydroxy-5′-methoxy-[2″,2″-(3″-hydroxy)-dimethylpyrano]-(5″,6″:3′,4′) flavanone (89) and Abyssinoflavanone IV (83) from the genus *Erythrina* as potential AChE inhibitors. MD simulation revealed the stability of both AChE–83 and AChE–89 complexes with RMSD of 1.525 ± 0.114 Å and 1.558 ± 0.126 Å, respectively. Both 83 and 89 exhibited lower binding energy compared to that of acetylcholine, further supporting the potency of 83 and 89 as AChE inhibitors. Moreover, DFT study suggested that both 83 and 89 exhibited higher E_{HOMO} and lower EA suggesting that both compounds were good electron donors compared to quercetin indicating that 89 and 83 could be potential radical scavengers through their electron-donating activity.

This study primarily relied on computational methods, the results could serve as s foundation to highlight the potency of 89 and 83 as both AChE inhibitors and free radical scavengers. Further investigation in wet laboratory experiments was warranted to validate their therapeutic potential for AD.

Acknowledgments

The authors are grateful to the University of Padjadjaran for providing funds through the Beasiswa Unggulan Pascasarjana Padjadjaran (BUPP) scheme and the Academic Leader Grant (ALG) by Tati Herlina (Grant Number 1549/UN6.3.1/PT.00.2023).

Disclosure

The author(s) report no conflicts of interest in this work.

References

1. Stanciu GD, Luca A, Rusu RN, et al. Alzheimer's disease pharmacotherapy in relation to cholinergic system involvement. *Biomolecules*. 2020;10(1). doi:10.3390/biom10010040
2. Jamal QMS, Khan MI, Alharbi AH, Ahmad V, Yadav BS. Identification of natural compounds of the apple as inhibitors against cholinesterase for the treatment of Alzheimer's disease: an in silico molecular docking simulation and ADMET Study. *Nutrients*. 2023;15(7):1579. doi:10.3390/nu15071579
3. Martins MM, Branco PS, Ferreira LM. Enhancing the therapeutic effect in Alzheimer's disease drugs: the role of polypharmacology and cholinesterase inhibitors. *ChemistrySelect*. 2023;8(10). doi:10.1002/slct.202300461
4. Ding Q, Shults NV, Gychka SG, Harris BT, Suzuki YJ. Protein expression of angiotensin-converting enzyme 2 (ACE2) is upregulated in brains with Alzheimer's disease. *Int J Mol Sci*. 2021;22(4):1687. doi:10.3390/ijms22041687
5. Vina J, LLoret A, Giraldo E, Badia C, Alonso M. Antioxidant pathways in Alzheimer's disease: possibilities of intervention. *Curr Pharm Des*. 2011;17(35):3861–3864. doi:10.2174/138161211798357755
6. Polidori MC, Mattioli P, Aldred S, et al. Plasma antioxidant status, immunoglobulin G oxidation and lipid peroxidation in demented patients: relevance to Alzheimer disease and vascular dementia. *Dement Geriatr Cognit Disord*. 2004;18(3–4):265–270. doi:10.1159/000080027
7. Mohamed HE, Abo-ELmatty DM, Mesbah NM, Saleh SM, Ali AMA, Sakr AT. Raspberry ketone preserved cholinergic activity and antioxidant defense in obesity induced Alzheimer disease in rats. *Biomed Pharmacother*. 2018;107. doi:10.1016/j.biopha.2018.08.034
8. Boasquívis PF, Silva GMM, Paiva FA, Cavalcanti RM, Nunez CV, De Paula Oliveira R. Guarana (Paullinia cupana) extract protects Caenorhabditis elegans models for Alzheimer disease and Huntington disease through activation of antioxidant and protein degradation pathways. *Oxid Med Cell Longev*. 2018;2018. doi:10.1155/2018/9241308
9. Mathew M, Subramanian S. In vitro screening for anti-cholinesterase and antioxidant activity of methanolic extracts of ayurvedic medicinal plants used for cognitive disorders. *PLoS One*. 2014;9(1):e86804. doi:10.1371/journal.pone.0086804

10. Ullah A, Munir S, Badshah SL, et al. Important flavonoids and their role as a therapeutic agent. *Molecules*. 2020;25(22):5243. doi:10.3390/molecules25225243
11. Lee VJ, Heffern MC. Structure-activity assessment of flavonoids as modulators of copper transport. *Front Chem*. 2022;10. doi:10.3389/fchem.2022.972198
12. Ghalloo BA, Khan KUR, Ahmad S, et al. Phytochemical profiling, in vitro biological activities, and in silico molecular docking studies of dracaena reflexa. *Molecules*. 2022;27(3):913. doi:10.3390/molecules27030913
13. Nazir N, Zahoor M, Nisar M, et al. Evaluation of neuroprotective and antiamnesic effects of Elaeagnus umbellata Thunb. On scopolamine-induced memory impairment in mice. *BMC Complement Med Ther*. 2020;20(1). doi:10.1186/s12906-020-02942-3
14. Dzoyem JP, Nkuete AHL, Ngameni B, Eloff JN. Anti-inflammatory and anticholinesterase activity of six flavonoids isolated from Polygonum and Dorstenia species. *Arch Pharm Res*. 2017;40(10):1129–1134. doi:10.1007/s12272-015-0612-9
15. Fahmy NM, Al-Sayed E, El-Shazly M, Singab AN. Comprehensive review on flavonoids biological activities of Erythrina plant species. *Ind Crops Prod*. 2018;123:500–538. doi:10.1016/j.indcrop.2018.06.028
16. Son NT, Elshamy AI. Flavonoids and other non-alkaloidal constituents of genus erythrina: phytochemical review. *Comb Chem High Throughput Screen*. 2021;24(1):20–58. doi:10.2174/1386207323666200609141517
17. Salem AM, Mostafa NM, Al-Sayed E, Fawzy IM, Singab ANB. Insights into the role of erythrina corallodendron L. in Alzheimer's disease: in vitro and in silico approach. *Chem Biodivers*. 2023;20(7). doi:10.1002/cbdv.202300200
18. Nassief SM, Amer ME, Shawky E, Saleh SR, El-Masry S. Acetylcholinesterase inhibitory alkaloids from the flowers and seeds of erythrina caffra. *Rev Bras Farmacogn*. 2020;30(6):859–864. doi:10.1007/s43450-020-00114-5
19. Santos WP, Da Silva Carvalho AC, Dos Santos Estevam C, Santana AEG, Marçal RM. In vitro and ex vivo anticholinesterase activities of Erythrina velutina leaf extracts. *Pharm Biol*. 2012;50(7):919–924. doi:10.3109/13880209.2011.649429
20. Patil VS, Meena H, Harish DR. Erythrina variegata L. bark: an untapped bioactive source harbouring therapeutic properties for the treatment of Alzheimer's disease. *Silico Pharmacol*. 2021;9(1). doi:10.1007/s40203-021-00110-0
21. Naqvi AAT, Mohammad T, Hasan GM, Hassan Md I. Advancements in docking and molecular dynamics simulations towards ligand-receptor interactions and structure-function relationships. *Curr Top Med Chem*. 2019;18(20). doi:10.2174/1568026618666181025114157
22. Akili Abd WR, Hardianto A, Latip J, Permana A, Herlina T. Virtual Screening and ADMET prediction to uncover the potency of flavonoids from genus erythrina as antibacterial agent through inhibition of bacterial ATPase DNA Gyrase B. *Molecules*. 2023;28(24):8010. doi:10.3390/molecules28248010
23. Hardianto A, Yusuf M, Hidayat IW, Ishmayana S, Soedjanaatmadja UMS. Exploring the Potency of *Nigella sativa* Seed in Inhibiting SARS-CoV-2 main protease using molecular docking and molecular dynamics simulations. *Indonesian J Chem*. 2021;21(5):1252. doi:10.22146/IJC.65951
24. Hardianto A, Mardetia SS, Destiarani W, Budiman YP, Kurnia D, Mayanti T. Unveiling the anti-cancer potential of onoceranoid triterpenes from lansium domesticum Corr. cv. kokosan: an in silico study against estrogen receptor alpha. *Int J Mol Sci*. 2023;24(19). doi:10.3390/ijms241915033
25. Deviani V, Hardianto A, Farabi K, Herlina T. Flavanones from erythrina crista-galli twigs and their antioxidant properties determined through in silico and in vitro studies. *Molecules*. 2022;27(18):6018. doi:10.3390/molecules27186018
26. Rouhani M. Evaluation of structural properties and antioxidant capacity of Proxison: a DFT investigation. *Comput Theor Chem*. 2021;1195. doi:10.1016/j.comptc.2020.113096
27. Azam F, Taban IM, Eid EEM, et al. An in-silico analysis of ivermectin interaction with potential SARS-CoV-2 targets and host nuclear importin α. *J Biomol Struct Dyn*. 2022;40(6):2851–2864. doi:10.1080/07391102.2020.1841028
28. Pantaleao SQ, Fernandes PO, Goncalves JE, Maltarollo VG, Honorio KM. Recent advances in the prediction of pharmacokinetics properties in drug design studies: a review. *ChemMedChem*. 2022;17(1–13). doi:10.1002/cmdc.202100542
29. Ghahremanian S, Rashidi MM, Raeisi K, Toghraie D. Molecular dynamics simulation approach for discovering potential inhibitors against SARS-CoV-2: a structural review. *J Mol Liq*. 2022;354. doi:10.1016/j.molliq.2022.118901
30. Liao Y, Mai X, Wu X, Hu X, Luo X, Zhang G. Exploring the inhibition of quercetin on acetylcholinesterase by multispectroscopic and in silico approaches and evaluation of its neuroprotective effects on PC12 cells. *Molecules*. 2022;27(22):7971. doi:10.3390/molecules27227971
31. Cob-Calan NN, Chi-Uluac LA, Ortiz-Chi F, et al. Molecular docking and dynamics simulation of protein β-tubulin and antifungal cyclic lipopeptides. *Molecules*. 2019;24(18):3387. doi:10.3390/molecules24183387
32. Tripathi N, Goel B, Bhardwaj N, Sahu B, Kumar H, Jain SK. Virtual screening and molecular simulation study of natural products database for lead identification of novel coronavirus main protease inhibitors. *J Biomol Struct Dyn*. 2022;40(8):3655–3667. doi:10.1080/07391102.2020.1848630
33. Ahmad SS, Khan MB, Ahmad K, et al. Biocomputational screening of natural compounds against acetylcholinesterase. *Molecules*. 2021;26(9):2641. doi:10.3390/molecules26092641
34. Ordentlich A, Barak D, Kronman C, et al. The architecture of human acetylcholinesterase active center probed by interactions with selected organophosphate inhibitors. *J Biol Chem*. 1996;271(20):11953–11962. doi:10.1074/jbc.271.20.11953
35. Álvarez-Berbel I, Espargaró A, Viayna A, et al. Three to tango: inhibitory effect of quercetin and apigenin on acetylcholinesterase, amyloid-β aggregation and acetylcholinesterase-amyloid interaction. *Pharmaceutics*. 2022;14(11):2342. doi:10.3390/pharmaceutics14112342
36. Fassihi A, Hasanzadeh F, Attar A, Saghaie L, Mohammadpour M. Synthesis and evaluation of antioxidant activity of some novel hydroxypyridinone derivatives: a DFT approach for explanation of their radical scavenging activity. *Res Pharm Sci*. 2020;15(6):515. doi:10.4103/1735-5362.301336
37. Karalis V, Macheras P, Van Peer A, Shah VP. Bioavailability and bioequivalence: focus on physiological factors and variability. *Pharm Res*. 2008;25:1956–1962. doi:10.1007/s11095-008-9645-9
38. Bittermann K, Goss KU. Predicting apparent passive permeability of Caco-2 and MDCK cell-monolayers: a mechanistic model. *PLoS One*. 2017;12(12):e0190319. doi:10.1371/journal.pone.0190319
39. Daly AK, Rettie AE, Fowler DM, Miners JO. Pharmacogenomics of CYP2C9: functional and clinical considerations. *J Pers Med*. 2018;8(1). doi:10.3390/jpm8010001